Geophysical Research Letters

RESEARCH LETTER
10.1029/2018GL080261

Climate Change Suppresses Santa Ana Winds of Southern California and Sharpens Their Seasonality

Janin Guzman-Morales[1] and **Alexander Gershunov**[1]

[1]Climate, Atmospheric Science and Physical Oceanography (CASPO) Research Division, Scripps Institution of Oceanography, University of California, San Diego, CA, USA

Key Points:
- GCMs project decreasing Santa Ana wind (SAW) activity in the 21st century
- The most pronounced reductions are projected to occur in early (fall) and late (spring): shoulders of the SAW season
- These reductions are due primarily to decreasing frequency of SAWs and much less so to their decreasing intensity

Supporting Information:
- Supporting Information S1

Correspondence to:
J. Guzman-Morales,
jguzmanmorales@ucsd.edu

Citation:
Guzman-Morales, J., & Gershunov, A. (2019). Climate change suppresses Santa Ana winds of Southern California and sharpens their seasonality. *Geophysical Research Letters*, *46*, 2772–2780. https://doi.org/10.1029/2018GL080261

Received 29 AUG 2018
Accepted 19 JAN 2019
Accepted article online 31 JAN 2019
Published online 5 MAR 2019

Abstract We downscale Santa Ana winds (SAWs) from eight global climate models (GCMs) and validate key aspects of their climatology over the historical period. We then assess SAW evolution and behavior through the 21st century, paying special attention to changes in their extreme occurrences. All GCMs project decreases in SAW activity, starting in the early 21st century, which are commensurate with decreases in the southwestward pressure gradient force that drives these winds. The trend is most pronounced in the early and late SAW season: fall and spring. It is mainly determined by changes in the frequency of SAW events, less so by changes in their intensity. The peak of the SAW season (November–December–January) is least affected by anthropogenic climate change in GCM projections.

Plain Language Summary Dry and gusty Santa Ana winds (SAWs) drive the most catastrophic wildfires in Southern California. Their sensitivity to the changing climate has been a matter of uncertainty and debate. We have assessed the response of SAW activity to global warming and describe these results in detail here. The overall decrease in SAW activity robustly projected by downscaled global climate models is strongest in the early and late seasons—fall and spring. SAWs are expected to decrease least at the peak of their season approximately December. Importantly, decreased SAW activity in the future climate is driven mainly by decreased frequency rather than the peak intensity of these winds. These results, together with what we know from recent literature about how precipitation is projected to change in this region, suggest a later wildfire season in the future.

1. Introduction

The wildfire season in coastal Southern California (SoCal: bounded by Southern California's Coast Ranges from the Transverse Ranges to the north to the Peninsular Ranges to the south) displays a unique seasonality. While the rest of western North America is mainly susceptible to wildfires during summer, SoCal's fire season peaks, historically, in the fall (Kolden & Abatzoglou, 2018). This timing results from a climatic coincidence of two seasonal factors: the long dry summer defining this Mediterranean climate regime and the dry gusty downslope winds, whose season starts in the fall when vegetation is at its seasonal driest. The Santa Ana winds (SAWs; Guzman-Morales et al., 2016; Hughes & Hall, 2010; Raphael, 2003), rooted in cold air masses over the elevated Great Basin, are notorious for fanning California's largest wildfires. SAW-fanned wildfires typically rage in the sloping coastal backcountry, with its encroaching wildland-urban-interface (WUI), where the gusty downslope SAWs are strongest (Guzman-Morales et al., 2016; Moritz et al., 2010) and ignitions are nearly always human caused (Kolden & Abatzoglou, 2018; Syphard & Keeley, 2015). While the local impacts of these wildfires are devastating (e.g., Medina, 2017), smoke blowing toward the densely populated coastal zone exposes much larger and diverse populations to remote respiratory health impacts (Delfino et al., 2009).

The largest wildfire in SoCal's recorded history, the Thomas Fire, was recently fanned by SAWs and raged through most of December 2017 into January 2018, until the first significant rains of the water year occurred, causing debris flows from the steep scorched landscape (Boyle, 2018; Oakley et al., 2018). Beyond the duration and magnitude of this fire, its most unusual feature was its December timing. Following a bone dry fall and early winter, the vegetation was desiccated in December 2017, allowing successive SAWs to fan the Thomas Fire. Although SAW activity peaks in December (Guzman-Morales et al., 2016), the vegetation is typically no longer as flammable by then as several rain storms would have normally occurred by that late into the wet season (Westerling et al., 2004). However, while enhancing extreme precipitation, climate change is projected to decrease the frequency of precipitation events in California (Polade et al., 2014,

2017), particularly in SoCal and especially in the shoulder seasons of fall and spring (Pierce et al., 2013). This is expected to result increasingly more often in dry flammable fuels persisting into the peak of the SAW season, therefore lengthening the wildfire season toward winter (Syphard et al., 2018). This reasoning is predicated on the assumption of no significant change in future SAW activity. In this work, we examine the validity of this assumption.

Guzman-Morales et al. (2016, hereafter GM'16) developed a historical 65-year catalog of hourly SAWs, validated them with available observations, analyzed their climatology and variability on different time scales, and identified potential sources of seasonal predictability. GM'16 detected SAWs purely from wind speed and direction. Although significant multidecadal variability was observed, this longest available record of SAWs did not manifest trends attributable to anthropogenic causes.

Two studies directly addressed changes of SAWs in future climate projections. These studies provided conflicting results. First, Miller and Schlegel (2006) assessed projected climatological monthly changes of SAW occurrences as detected using large-scale pressure gradient in two Climate Model Intercomparison Project, Phase 3 (CMIP3; Meehl et al., 2007) global climate models (GCMs) forced by low (B1) and high (A2) emission scenarios. Their results suggested a decline of SAW occurrences in September but a significant increase in December, at the peak of the SAW season, in the last 30 years of the 21st century relative to the equivalent period of the 20th century. However, large variation in those results was identified in the early and middle parts of the 21st century between models and emission scenarios. The second study by Hughes et al. (2011) used one dynamically downscaled CMIP3-generation GCM under the A1B emission scenario to generate a local gap-flow-based projection of SAWs. This study reported an all-season (October–March) mean decrease of ~20% in the number of annual Santa Ana days by mid-21st century, of which only October and February had a statistically significant change. This anthropogenic change was attributed to the disproportionate warming of the cold pool of air over the Great Basin relative to that of the coastal marine air mass, attenuating the potential temperature gradient between the Great Basin and the Pacific Ocean off the coast of California, which is an important thermodynamic mechanism for the formation of SAWs (Hughes & Hall, 2010). Additionally, two related studies, Yue et al. (2014) and Jin et al. (2015) addressed the SoCal wildfire regime change, explicitly estimating changes in temperature, precipitation, humidity, and SAWs as climatic drivers for 21st century projections of increased total burned area. Their results were obtained with different methods applied to different sets of GCMs and CMIP experiments, but were only partially due to increased SAW activity in the fall.

The inconsistencies and incompatibilities in projected SAW trends over the 21st century identified by the abovementioned studies seem to arise, at least partially, from differences in the approach used to define, detect, and downscale SAWs as well as from the limited choice of GCMs in some studies. In this work, we construct future projections of SAWs based on a dynamically trained statistical downscaling of daily winds over the SoCal domain in a set of eight GCMs. In addition to their prior validation over California, we validate these GCMs, with respect to their ability to reproduce key features of SAW (sections 3.1 and 3.2). Using these downscaled GCMs, we provide a description of future SAW behavior focusing on changes in SAW activity, reflecting changes in frequency, intensity, and seasonality, as well as in extreme SAW events (section 3.3). We then examine the synoptic cause of projected SAW trends—trends in the pressure gradient (section 3.3) and conclude by discussing results in the context of SoCal's changing wildfire regime (section 4).

2. Data and Methods

2.1. Downscaling Santa Ana Winds: A Summary

We utilize coarse-resolution winds from National Centers for Environmental Prediction/National Center for Atmospheric Research Global Reanalysis 1 (R1; Kalnay et al., 1996) and dynamical downscaled winds from the California Reanalysis Downscaling at 10 km (CaRD10; Kanamaru & Kanamitsu, 2007; Kanamitsu & Kanamaru, 2007) to train the statistical downscaling of winds to a 10 × 10-km grid. The mesoscale CaRD10 product is the explicit dynamical translation of R1 large-scale circulation via the Regional Spectral Model (Kanamaru et al., 2005).

Prior to the statistical downscaling of fine-resolution winds, we use Canonical Correlation Analysis (Hotelling, 1935) in its diagnostic mode (Guirguis et al., 2014; Roca & Gershunov, 2004; Schwartz et al., 2014), to extract the relevant patterns of association (*Canonical Correlates*, CCs) between coarse- (R1) and fine- (CaRD10) resolution winds. Then, we examined the variability explained by the CCs as well as their resemblance with SoCal wind regimes (Conil & Hall, 2006). Subsequently, the statistical downscaling model was constructed and optimized based on the prognostic application of Canonical Correlation Analysis (Alfaro et al., 2006; Barnett & Preisendorfer, 1987; García-Bustamante et al., 2012; Gershunov & Cayan, 2003) to the R1 (predictor) and CaRD10 (predictand) wind fields.

The dynamically trained statistical downscaling approach, statistical model optimization, downscaled historical daily vector wind fields over SoCal, and their validation are described in detail in supporting information sections S1–S4. We refer to this downscaling of R1 winds as *R1D*. Extending the SAW detection methodology of GM'16 to daily winds and applying it to wind vectors thus downscaled onto the 10 × 10-km CaRD10 grid from R1 is also described in supporting information section S5. We then downscaled daily winds from historical and RCP8.5 future GCM surface winds regridded to the R1 grid over SoCal and derived SAWs from them in a similar manner. These local SAWs were summarized regionally as the Santa Ana Wind Regional Index (SAWRI). SAWRI is the daily mean SAW speed computed over the grid cells within the SAW domain (GM'16) and therefore is expressed in meters per second. For complete description of local SAW detection and SAWRI derivation, see GM'16. Unless otherwise stated, although 10 × 10-km gridded SAWs are available, in what follows, we quantify Santa Ana wind activity using SAWRI.

2.2. Selection and Validation of GCMs

The eight GCMs (Table S1) were those providing the requisite daily data among the 10 GCMs previously selected, from a total of 31 CMIP5 GCMs, for their realism in reproducing several key features of the California climate (Lynn et al., 2015). We then assessed the GCMs' ability to reproduce SAWRI by quantifying its behavior, for example, frequency, intensity, seasonality, timing, and sensitivity to its synoptic driver—the pressure gradient force (PGF)—over the historical period by comparison to SAWRI derived from R1D and CaRD10 winds. Table S1 summarizes these validation results for the eight GCMs, which are discussed in section 3.2. The validation helps us to interpret anthropogenic trends in projected SAW activity. Unless otherwise stated, *SAW Activity* is defined as the accumulation of SAWRI over the relevant period in question (e.g., month, year). We focus on projected changes occurring in two time periods: the first and second halves of the 21st century, 2000–2049 and 2050–2099, respectively, relative to the last half of the 20th century, 1950–1999.

2.3. Quantifying SAW Sensitivity to the Synoptic Pressure Gradient Force

We computed daily sea level pressure (SLP) anomalies in the synoptic domain for R1 and GCM data sets during the historical validation period shared by R1 and the GCMs (1950–2005). Associated pressure gradient force (PGF) fields were derived as the negative of the SLP gradient in the x and y direction:

$$PGF_{xy} = PGF_x + PGF_y = -\sqrt{\frac{\Delta p^2}{\Delta x} + \frac{\Delta p^2}{\Delta y}}$$

We composited SLP and PGF fields on SAW days as identified by SAWRI in the corresponding R1 and GCM products (Figure 1). Further, we produced maps of correlations between SAWRI and the PGF evaluated geographically (Figure S1). The resultant vector correlation at each grid cell in the large-scale domain is calculated as the vector sum of the SAWRI correlations with the PGF components in the x and y (Lon and Lat) directions:

$$r_{PGFxy,SAWRI} = \sqrt{r_{PGFx,SAWRI}{}^2 + r_{PFGy,SAWRI}{}^2}$$

The subregion where $r_{PGFxy,\ SAWRI}$ values are above the 95th percentile of correlations across the synoptic domain is continuous, coincides well with SAW geographically, and defines the region of maximum PGF-SAW association in all data sets (highlighted in red arrows on Figure S1). The spatial mean correlation in this subregion is 0.72 in the R1 data set and ranges from 0.65 to 0.92 in GCMs (Figure S1). Daily average

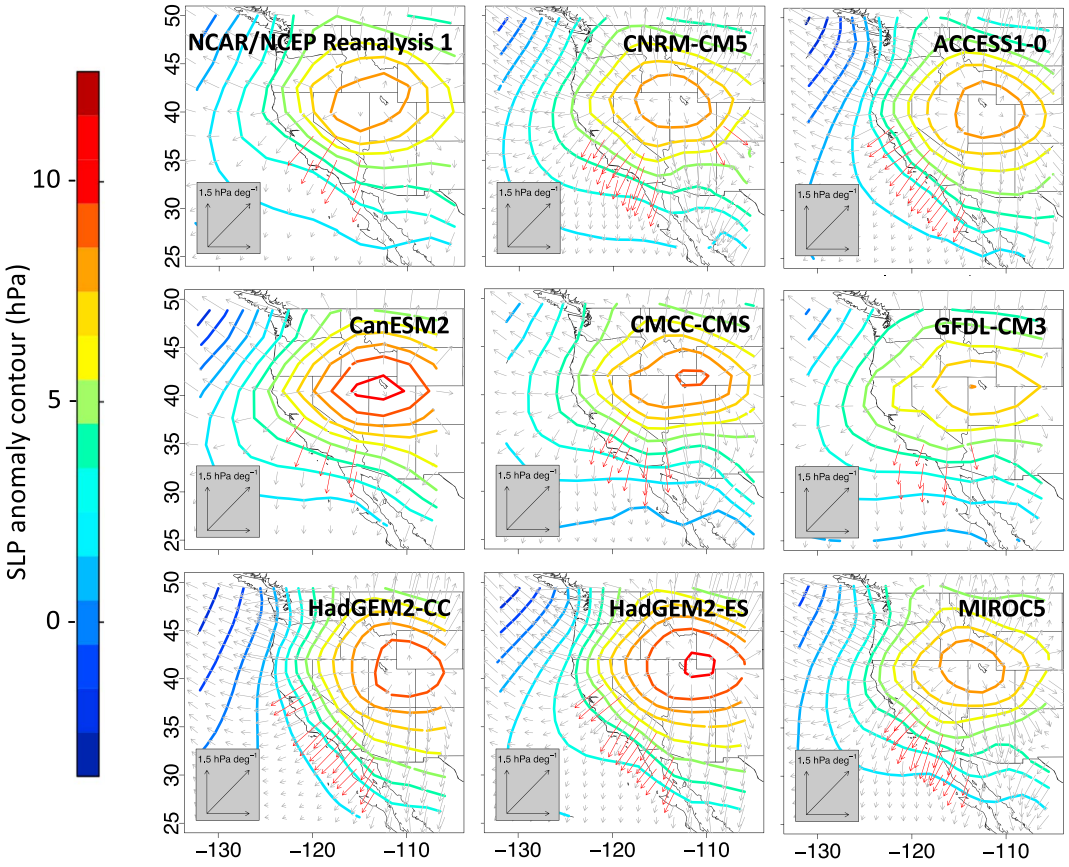

Figure 1. Sea level pressure (SLP) and pressure gradient force (PGF) composite anomaly maps during Santa Ana Wind days. Contour lines delineate SLP anomalies, while gray arrows indicate associated PGF field. Red arrows mark the region where correlation between PGF and Santa Ana Wind Regional Index is above the 95th percentile as shown in Figure S1 in the supporting information. NCAR = National Center for Atmospheric Research; NCEP = National Centers for Environmental Prediction.

PGF over this SAW-relevant subregion (PGF_{r95}) was retrieved for every SAW day in the historical validation period. We then linearly related SAWRI and PGF_{r95}.

3. Results

3.1. SAW Sensitivity to Synoptic Pressure Patterns

The SLP composite of SAW days from R1 shows a high-pressure anomaly located over the northeastern fringes of the Great Basin, centered at the intersection of Nevada, Utah, and Idaho (Figure 1, top left), traditionally considered the signature large-scale SLP forcing of SAWs (Abatzoglou et al., 2013; Raphael, 2003; Sommers, 1978). This SLP anomaly creates a southwestward PGF field over a region that covers most of California, expanding from the San Francisco Bay Area to Northern Baja California. The average PGF_{r95} (highlighted in red arrows on Figure 1) during all SAW days amounts to 91 Pa/deg. Deriving downslope SAWs from large-scale circulation, that is, PGF, would require consideration of air masses, topography, vertical katabatic acceleration, and friction terms; here, instead, we intend to develop a quantitative relationship between a metric derived from large-scale SLP anomaly patterns and regionally-averaged SAWs based on simplified synoptic-scale forcing considerations, that is, circulation features that may be affected by climate change.

All eight models reasonably reproduce a realistic SLP composite anomaly pattern and associated northeasterly PGF field over the relevant regional domain, that is, California and Northern Baja California (Figure 1) during SAW days. The composite SLP anomaly shape variation between GCMs seems responsible for the

variations in PGF directions over the area of high correlations (r_{95}). Despite these differences, the mean PGF_{r95} associated with the SLP anomaly in GCMs is comparable (77.1–95.2 Pa/deg) to that manifest in R1 (91 Pa/deg).

The pressure gradient force (PGF_{r95}) explains 68% ($r = 0.83$) of the daily variability of SAWRI in the R1 data set and between 40% and 67% ($0.63 < r < 0.82$) in GCMs. The linear fit between SAWRI and PGF_{r95} is shown in Figure S2, and the associated correlation coefficients and slopes are summarized in Table S1. The quantitative evaluation of SAWRI sensitivity to PGF in GCMs relative to R1 is further discussed in section 3.2, whereas the SAWRI versus PGF_{r95} changes in the 21st century are addressed in section 3.3.

3.2. GCMs' Downscaled Performance in Reproducing SAWs

We follow in the footsteps of previous studies that assessed GCM ability to simulate synoptic weather features (e.g., Gershunov & Guirguis, 2012; Payne & Magnusdottir, 2015). No GCM can be considered "best" for realistically capturing all SAW features evaluated here. With respect to total seasonal SAW activity, CNRM-CM5, CMCC-CSM, ACCESS1–0, and HadGEM2-ES have negative bias, whereas CanESM2, GDFLCM-3, HadGEM2-CC, and MIROC5 yield larger positive bias relative to R1 (Figure S3a). A closer examination of SAW frequency and wind speed (or *intensity*, as summarized by SAWRI), which together define total seasonal SAW activity, allows us to identify sources of bias in seasonal SAW activity for each GCM. All models overestimate the frequency of SAW days but vary on the sign of intensity error (Figure S3b and Table S1). CNRM-CM5 and CMCC-CSM overestimate frequency and underestimate SAWRI by a similar degree yielding the closest mean total annual SAW activity and associated interannual variability compared to R1 (see whiskers on Figure S3a). ACCESS1–0 and HadGEM2-ES show larger underestimations of SAWRI (−32% in both cases), corresponding to a larger negative bias in total annual SAW activity. By contrast, the positive bias of SAW activity from GDFL-CM3 and HadGEM2-CC is dominated by the overestimation of SAW frequency, while intensity errors are remarkably small. Finally, CanESM2 and MIROC display the least realistic performance with the highest overestimations of SAW frequency and intensity, which result in the largest positive errors in annual SAW activity.

All GCMs generally reproduce SAW seasonality: monthly SAW activity ramping up through fall, peaking in winter, and gradually declining by late spring (Figure S3c). All GCMs manifest no or negligible SAW activity over summer. ACCESS1–0 and HadGEM2-ES display the most realistic seasonal cycle with the smallest monthly SAW activity difference relative to R1D (21 and 18.5 m/s, respectively), estimated as the root sum of squared differences across all months. By breaking down seasonal total SAW activity, again into frequency and intensity, we observe that the amplitude differences in seasonality are dominated by wind speed errors (Figure S4d), while deviation in shape is better explained by frequency errors (Figure S4c). This is, for example, the case for the overestimation of SAW activity in fall for CMCC-CMS and GDFL-CM3. According to R1D, the annual maximum SAW day tends to occur on December 31 ± 29 (1 standard deviation) days (Figure 3d). CNRM-CM5, and MIROC5 yield the closest timing falling within two days of what is recorded historically, but display a larger spread.

In terms of SAWRI sensitivity to daily variations in PGF, HadGEM2-CC, HadGEM2-ES, and CanESM2 display the highest and most realistic correlations, with the PGF explaining between 60% and 67% of the daily SAWRI variance. Differences in the linear fit slope (Table S1) show that HadGEM2-CC and GDFL-CM3 detect the most realistic magnitude of SAWRI response to PGF_{r95} variability, while HadGEM2-ES and ACCESS1–0 have the highest underestimation of the effect of PGF variations on SAWRI (flattest slopes).

In summary, there are no clear winners or losers among the models. Therefore, it is difficult to highlight a subset of these eight GCMs when we consider projected changes in SAWs. Results of these validation exercises, however, will help interpret elements of projected SAW changes by illuminating individual model idiosyncrasies.

3.3. Projections of SAWs Through the 21st Century

GCMs project a decrease of total seasonal SAW activity starting during the first half of the 21st century (Figure S5) and continuing during the last half century, when the reduction of SAW activity is projected to be −18.5% ± 4.5% (mean change ±1 sd) on seasonal average. Meanwhile, the decrease of extreme SAW activity (the strongest 10% of events) is about twice as large (−34.3% ± 9.2%); see Figure 2a. The reduction

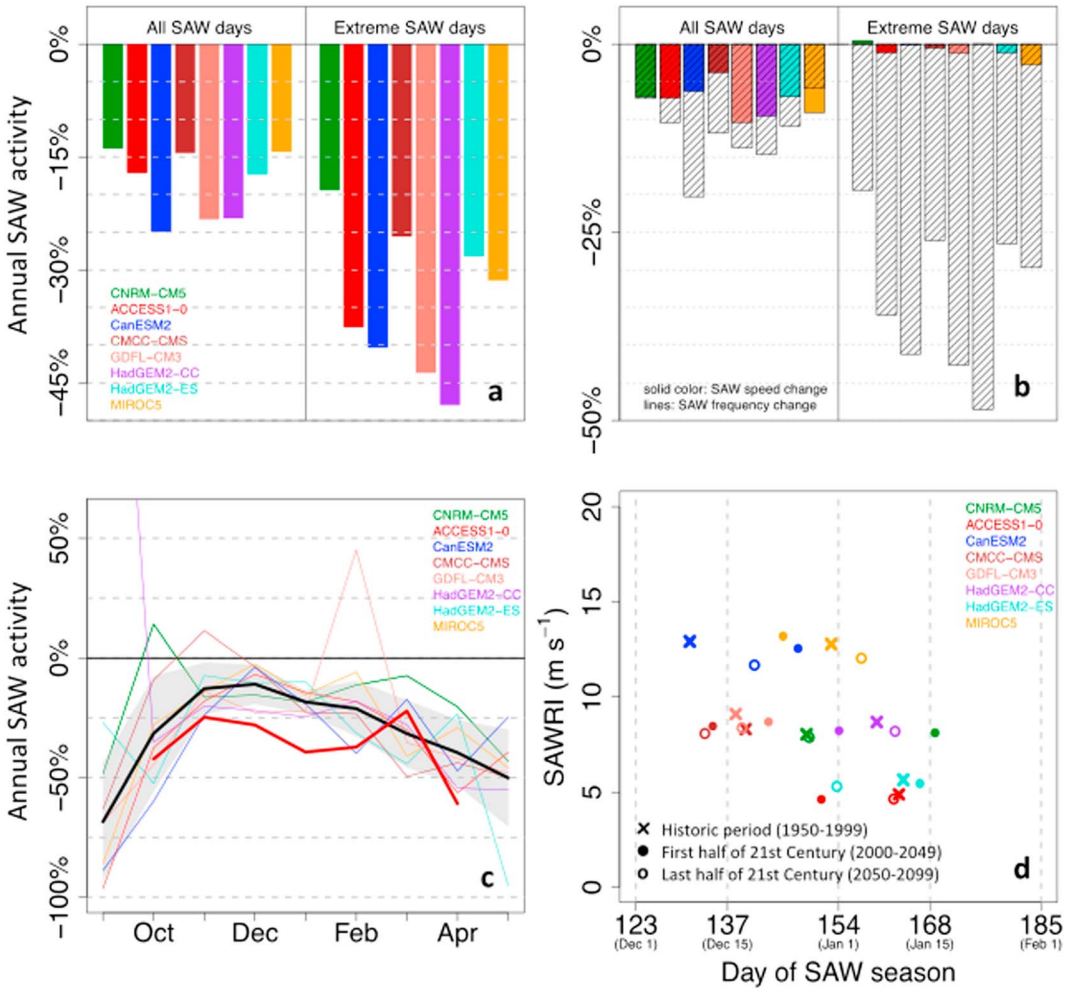

Figure 2. Future projection of Santa Ana Wind (SAW) features. Changes are for the last half of the 21st century (2045–2099) and are relative to the base historical period (1950–1999). (a) Percentage change of total seasonal SAW activity for all SAW days (left) and extreme SAW days (right). (b) Percentage change of wind speed and frequency for all SAW days (left) and extremes SAW days (right). (c) Percentage change of the SAW run seasonality. Thick black line shows the global climate model ensemble mean and gray envelopes delineate ±1 standard deviation. Thick red line corresponds to the all global climate models mean change of extreme SAWs. (d) Timing of maximum annual SAW day. Changes for both the first and last halves of the 21st century are included in panel (d).

of SAW activity is explained by a larger reduction in SAW frequency than that in wind speed, according to most models (Figure 2b). This is especially true for extreme SAWs, where the reduction in intensity is very small (−0.81% ± 0.99%) relative to the reduction in frequency (−33.8% ± 9.9%).

In terms of seasonality, reduction of SAW activity is robust across all months and all GCMs (Figure 2c) with very few exceptions: HadGEM2-CC, CNRM-CM5, CMCC-CMS, and GDFL-CM3 show increases of SAW activity in September (+273%), October (+14%), November (+11%), and February (+45%), respectively. However, the actual SAW activity detected in HadGEM2-CC in September and in GDFL-CM3 in February is severely underestimated compared to the R1D historical record (Figure S3c), inflating any changes expressed relative to climatology.

The GCM ensemble suggests that November, December, and January are projected to experience the smallest decreases in SAW activity, in that order. Specifically, the following changes are projected (given as the GCM ensemble mean ±1 sd): −5% ± 10% and −13% ± 11% for the first and second halves of the 21st century, respectively, in November; −4% ± 8% and −11% ± 8% in December, and −12% ± 5% and −18% ± 5% in January. Greater changes are projected for the tails of the SAW season, when, by the second half of the

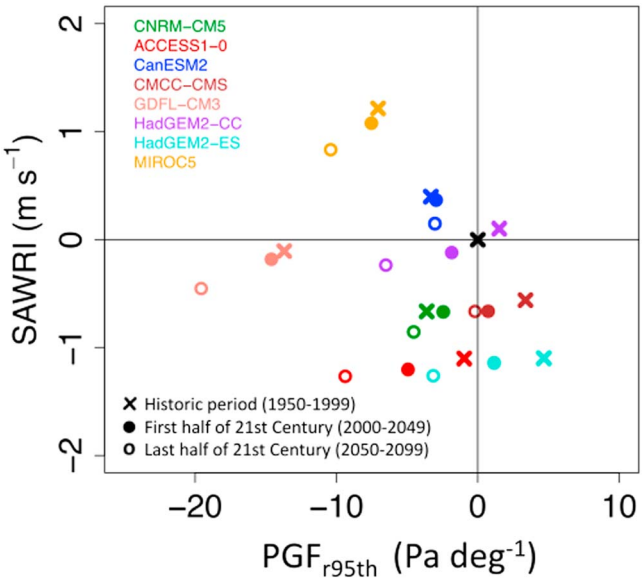

Figure 3. Santa Ana wind sensitivity to changes in pressure gradient force. Crosses are differences with respect to R1D historical mean (black cross at the origin). Full and empty circles denote changes projected for the first and second halves of the 21st century, respectively. SAWRI = Santa Ana Wind Regional Index.

century, the average reduction reaches −32 ± 24% (October) and −32% ± 14% (March) with a larger decrease in early season (September–October) compared to late season (March–May). For extreme SAWs, we find a more pronounced decrease overall with similar proportional distribution across the season, that is, smallest decreases around the peak season in November and December (−25%) with greater decreases early and late in the season (Figure 2c). Our results are in general agreement with those of Hughes et al. (2011) who showed a stronger decrease in SAW frequency at the shoulders of their season (October and February) and an insignificant increase in January.

We find no agreement among GCMs regarding changes in mean timing of annual maximum SAW day (Figure 2d), where the annual maximum SAW day refers to the day with the highest regional wind speed of the season as given by SAWRI. GCMs do not show consistent model-to-model changes toward a specific time of the season or consistent within-model tendency for the first and last half of the 21st century. It is noteworthy, however; that the strength of the maximum annual SAW day shows a very modest average decrease (−1.7% ± 2.9% and −5.4% ± 2.2%, during the first and second halves of the century, respectively, (GCM ensemble mean ±1 sd) consistent with smaller wind speed reductions projected for extreme SAWs as compared with average SAWs.

Lastly, for all GCMs, except CanESM2, the projected decrease in SAWRI is associated with a decrease of PGF_{r95} regardless of the specific SAWRI-PGF_{r95} sensitivity (Figure 3). SAW-associated PGF is not projected to clearly decrease in that model, while SAW activity slightly decreases regardless. The other GCMs show a remarkable consistency in the cause of projected decreases in SAW activity.

4. Discussion and Conclusions

In general, we found the ability of downscaled GCMs to represent SAWs to be reasonable overall, but some models displayed serious problems with specific features of SAWs. Nonetheless, the agreement between models on projected SAW changes was rather striking. We note that our study was limited to wind speed and direction only. The other salient features of SAWs—humidity and temperature—were not considered here. For winds, however, our results provide a consistent picture that provides important nuance heretofore unavailable.

Overall, GCMs agree on the gradual decrease in SAW activity, particularly in the shoulder seasons of fall and spring. The decrease in SAW activity is least pronounced during the winter peak of the SAW season. This decrease, which appears to be gradual, that is, monotonic during the first and second halves of the 21st century, but not yet clearly evident in the 20th century, is driven by a decreased PGF that is associated with SAWs. This result is generally consistent with the conclusion of Hughes et al. (2011), who project decreased SAW frequency as a result of the greater warming projected over the Great Basin compared to that over the northeastern Pacific Ocean. We further find that the decrease in SAW activity is driven most strongly and consistently by decreased *frequency* of SAWs, particularly in the shoulder seasons. Projected intensity, that is, wind speed, also tends to decrease consistently, but to a much lesser degree. This is especially true for extreme SAWs, whose frequency is projected to decrease strongly (by 34 ± 10%, i.e., mean ±1 sd) by the last half of the 21st century, but whose intensity is hardly projected to change.

A robust result that is salient for the timing of the wildfire season is that the SAW season is narrowing around its natural peak in December, when changes in SAW activity are projected to be minimal (−4% ± 8% and −11% ± 8%, for the first and second halves of the 21st century, respectively). November and January SAWs are also projected to become somewhat less active: by −5% ± 10% and −13% ± 11% in November, and by −12% ± 5% and −18% ± 5% in January. The strongest decreases in SAW activity are projected for the early SAW season (68% and 30%, respectively, on ensemble average for September and October in the second half of the century) and for the late season (35% in April and 50% in May). The expectation,

therefore, is that climate change may result in a weakening contribution of SAWs to the traditional SoCal wildfire season's October peak. However, we may expect an increase in late-season, November–December–January, wildfires given the projected minimum decrease of SAW activity during this traditional peak of the SAW season and the independent projection of decreased fall precipitation (Pierce et al., 2013; Swain et al., 2018). Importantly, the intensity of extreme SAWs during the peak of the SAW season is not really expected to diminish. The slightly diminished SAWs (mainly in their frequency) in December, for example, will still tend to be stronger and more frequent in the late 21st century compared to historical SAWs in October, the historical peak of the wildfire season. In other words, the projected precipitation regime and SAW changes suggest a tendency for migration of the SoCal wildfire season peak from October toward December. Similar projected changes in precipitation and SAW regimes likely reflect the influence of poleward expanding subtropical subsidence (Previdi & Liepert, 2007; Quan et al., 2014), which pushes synoptic activity—that drives both precipitation and SAWs—poleward, particularly in the shoulder seasons.

In light of these projections, the largest wildfire in SoCal history (Thomas Fire) occurring in December 2017 and fanned by back-to-back SAW events is likely a harbinger of wildfire seasonality we would expect to experience more often in the future. In December, back-to-back SAWs are most probable providing opportunities for wildfires to burn longer and bigger. In the future, the probability of back-to-back events will diminish somewhat, but will still remain much stronger in December than it ever was in October or even November. The higher year-to-year precipitation volatility (Polade et al., 2014) translates into higher probability of extremely wet winters followed by extremely dry winters (Swain et al., 2018) and additionally suggests a boost to the availability of dry fuels, bolstering the later peak in future wildfire activity, that is, nudging the extremes of future later fires to be more intense and, therefore, more extensive. On the other hand, the progressively less frequent SAWs in early to middle fall (September–October) would result in less fuel desiccation via SAWs themselves, which remains to be quantified. Obviously, the above expectations about anthropogenically driven changes in future wildfire activity need to be evaluated in a more robust framework involving precipitation and SAW projections including humidity and temperature, in addition to projected ecosystem changes, as well as population and wildland-urban-interface dynamics, all as comprehensive inputs into wildfire risk models. Such comprehensive models could then be used to test our hypotheses about the future of wildfire seasonality and dynamics in SoCal as well as to begin assessing future impacts of wildfires on society.

Acknowledgments

Authors conducted this work funded by University of California Office of the President MRPI grant MRP-17-446315 and the Climate Education Partners (www.sandiego.edu/climate), a NSF-funded project DUE-1239797. CONACYT-UCMEXUS doctoral fellowship (http://ucmexus.ucr.edu/) contributed with financial support for Janin Guzman-Morales (scholar 214550). Additional support was provided by the California Energy Commission EPC-16-093 and the U.S. Geological Survey grant G14AP00076. This study also contributes to DOI's Southwest Climate Science Center activities and NOAA's California and Nevada Applications Program award NA11OAR43101. We thank Dan Cayan and David Pierce for stimulating discussions and CMIP5 for compiling and providing data from GCM simulations. We are also thankful to three anonymous reviewers for their constructive feedback on the original manuscript. Lastly, we would like to mention and honor the bright memory of Masao Kanamitsu, creator of CaRD10. Data sets are available here http://dx.doi.org/10.17632/xvp7v9rt6k.1.

References

Abatzoglou, J. T., Barbero, R., & Nauslar, N. J. (2013). Diagnosing Santa Ana winds in Southern California with synoptic-scale analysis. *Weather and Forecasting*, *28*(3), 704–710. https://doi.org/10.1175/WAF-D-13-00002.1

Alfaro, E. J., Gershunov, A., & Cayan, D. (2006). Prediction of summer maximum and minimum temperature over the central and western United States: The roles of soil moisture and sea surface temperature. *Journal of Climate*, *19*(8), 1407–1421. https://doi.org/10.1175/JCLI3665.1

Barnett, T. P., & Preisendorfer, R. (1987). Origins and levels of monthly and seasonal forecast skill for United States surface air temperatures determined by canonical correlation analysis. *Monthly Weather Review*, *115*(9), 1825–1850. https://doi.org/10.1175/1520-0493(1987)115<1825:OALOMA>2.0.CO;2

Boyle T. C. (2018). The absence in Montecito. The New Yorker. Retrieved from https://www.newyorker.com/culture/cultural-comment/after-the-mudslides-an-absence-in-montecito

Conil, S., & Hall, A. (2006). Local regimes of atmospheric variability: A case study of Southern California. *Journal of Climate*, *19*(17), 4308–4325. https://doi.org/10.1175/JCLI3837.1

Delfino, R. J., Brummel, S., Wu, J., Stern, H., Ostro, B., Lipsett, M., et al. (2009). The relationship of respiratory and cardiovascular hospital admissions to the southern California wildfires of 2003. *Occupational and Environmental Medicine*, *66*(3), 189–197. https://doi.org/10.1136/oem.2008.041376

García-Bustamante, E., González-Rouco, J. F., Navarro, J., Xoplaki, E., Jiménez, P. A., & Montávez, J. P. (2012). North Atlantic atmospheric circulation and surface wind in the northeast of the Iberian Peninsula: Uncertainty and long term downscaled variability. *Climate Dynamics*, *38*(1–2), 141–160. https://doi.org/10.1007/s00382-010-0969-x

Gershunov, A., & Cayan, D. R. (2003). Heavy daily precipitation frequency over the contiguous United States: Sources of climatic variability and seasonal predictability. *Journal of Climate*, *16*(16), 2752–2765. https://doi.org/10.1175/1520-0442(2003)016<2752:HDPFOT>2.0.CO;2

Gershunov, A., & Guirguis, K. (2012). California heat waves in the present and future. *Geophysical Research Letters*, *39*, L18710. https://doi.org/10.1029/2012GL052979

Guirguis, K., Gershunov, A., Tardy, A., & Basu, R. (2014). The impact of recent heat waves on human health in California. *Journal of Applied Meteorology and Climatology*, *53*(1), 3–19. https://doi.org/10.1175/JAMC-D-13-0130.1

Guzman-Morales, J., Gershunov, A., Theiss, J., Li, H., & Cayan, D. (2016). Santa Ana winds of Southern California: Their climatology, extremes, and behavior spanning six and a half decades. *Geophysical Research Letters*, *43*, 2827–2834. https://doi.org/10.1002/2016GL067887

Hotelling, H. (1935). The most predictable criterion. *Journal of Educational Psychology*, *26*(2), 139–142. https://doi.org/10.1037/h0058165
Hughes, M., & Hall, A. (2010). Local and synoptic mechanisms causing Southern California's Santa Ana winds. *Climate Dynamics*, *34*(6), 847–857. https://doi.org/10.1007/s00382-009-0650-4
Hughes, M., Hall, A., & Kim, J. (2011). Human-induced changes in wind, temperature and relative humidity during Santa Ana events. *Climatic Change*, *109*(S1), 119–132. https://doi.org/10.1007/s10584-011-0300-9
Jin, Y., Goulden, M. L., Faivre, N., Veraverbeke, S., Sun, F., Hall, A., et al. (2015). Identification of two distinct fire regimes in Southern California: Implications for economic impact and future change. *Environmental Research Letters*, *10*(9), 94005. https://doi.org/10.1088/1748-9326/10/9/094005
Kalnay, E., Kanamitsu, M., Kistler, R., Collins, W., Deaven, D., Gandin, L., et al. (1996). The NCEP/NCAR 40-year reanalysis project. *Bulletin of the American Meteorological Society*, *77*(3), 437–471. https://doi.org/10.1175/1520-0477(1996)077<0437:TNYRP>2.0.CO;2
Kanamaru, H., Cui Y., & Juang H. (2005). Parallel implementation of the regional spectral atmospheric model. PIER Project Rep. CEC-500-2005-014. Retrieved from https://www.energy.ca.gov/2005publications/CEC-500-2005-014/CEC-500-2005-014.PDF
Kanamaru, H., & Kanamitsu, M. (2007). Fifty-seven-year California reanalysis downscaling at 10 km (CaRD10). Part II: Comparison with north American regional reanalysis. *Journal of Climate*, *20*(22), 5572–5592. https://doi.org/10.1175/2007JCLI1522.1
Kanamitsu, M., & Kanamaru, H. (2007). Fifty-seven-year California reanalysis downscaling at 10 km (CaRD10). Part I: System detail and validation with observations. *Journal of Climate*, *20*(22), 5553–5571. https://doi.org/10.1175/2007JCLI1482.1
Kolden, C., & Abatzoglou, J. (2018). Spatial distribution of wildfires ignited under katabatic versus non-katabatic winds in Mediterranean Southern California USA. *Fire*, *1*(2), 19. https://doi.org/10.3390/fire1020019
Lynn, E., Schwarz, A., Anderson, J., & Correa, M. (2015). Perspectives and Guidance for Climate Change Analysis. Climate Change Technical Advisory Group, California Department of Water Resources. Retrieved from http://climate.calcommons.org/bib/perspectives-and-guidance-climate-change-analysis
Medina, J. (2017). Scenes of devastation from California's latest wildfire. *The New York Times*, https://www.nytimes.com/2017/12/05/us/california-wildfire-ventura.html
Meehl, G. A., Covey, C., Delworth, T., Latif, M., McAvaney, B., Mitchell, J. F. B., et al. (2007). The WCRP CMIP3 multimodel dataset: A new era in climate change research. *Bulletin of the American Meteorological Society*, *88*(9), 1383–1394. https://doi.org/10.1175/BAMS-88-9-1383
Miller, N. L., & Schlegel, N. J. (2006). Climate change projected fire weather sensitivity: California Santa Ana wind occurrence. *Geophysical Research Letters*, *33*, L15711. https://doi.org/10.1029/2006GL025808
Moritz, M. A., Moody, T. J., Krawchuk, M. A., Hughes, M., & Hall, A. (2010). Spatial variation in extreme winds predicts large wildfire locations in chaparral ecosystems. *Geophysical Research Letters*, *37*, L04801. https://doi.org/10.1029/2009GL041735
Oakley, N. S., Cannon, F., Munroe, R., Lancaster, J. T., Gomberg, D., & Ralph, F. M. (2018). Brief communication: Meteorological and climatological conditions associated with the 9 January 2018 post-fire debris flows in Montecito and Carpinteria California, USA. *Natural Hazards and Earth Systems Science Discussions* https://doi.org/10.5194/nhess-2018-179, 1–11.
Payne, A. E., & Magnusdottir, G. (2015). An evaluation of atmospheric rivers over the North Pacific in CMIP5 and their response to warming under RCP 8.5. *Journal of Geophysical Research: Atmospheres*, *120*, 11,173–11,190. https://doi.org/10.1002/2015JD023586
Pierce, D. W., Das, T., Cayan, D. R., Maurer, E. P., Miller, N. L., Bao, Y., et al. (2013). Probabilistic estimates of future changes in California temperature and precipitation using statistical and dynamical downscaling. *Climate Dynamics*, *40*(3–4), 839–856. https://doi.org/10.1007/s00382-012-1337-9
Polade, S. D., Gershunov, A., Cayan, D. R., Dettinger, M. D., & Pierce, D. W. (2017). Precipitation in a warming world: Assessing projected hydro-climate changes in California and other Mediterranean climate regions. *Scientific Reports*, *7*(1), 10783. https://doi.org/10.1038/s41598-017-11285-y
Polade, S. D., Pierce, D. W., Cayan, D. R., Gershunov, A., & Dettinger, M. D. (2014). The key role of dry days in changing regional climate and precipitation regimes. *Scientific Reports*, *4*(1), 4364. https://doi.org/10.1038/srep04364
Previdi, M., & Liepert, B. G. (2007). Annular modes and Hadley cell expansion under global warming. *Geophysical Research Letters*, *34*, L22701. https://doi.org/10.1029/2007GL031243
Quan, X.-W., Hoerling, M. P., Perlwitz, J., Diaz, H. F., & Xu, T. (2014). How fast are the tropics expanding? *Journal of Climate*, *27*(5), 1999–2013. https://doi.org/10.1175/JCLI-D-13-00287.1
Raphael, M. N. (2003). The Santa Ana winds of California. *Earth Interactions*, *7*(8), 1–13. https://doi.org/10.1175/1087-3562(2003)007<0001:TSAWOC>2.0.CO;2
Roca, R., & Gershunov, A. (2004). Coupling of latent heat flux and the greenhouse effect by large-scale tropical/subtropical dynamics diagnosed in a set of observations and model simulations. *Climate Dynamics*, *22*(2–3), 205–222. https://doi.org/10.1007/s00382-003-0376-7
Schwartz, R. E., Gershunov, A., Iacobellis, S. F., & Cayan, D. R. (2014). North American west coast summer low cloudiness: Broadscale variability associated with sea surface temperature. *Geophysical Research Letters*, *41*, 3307–3314. https://doi.org/10.1002/2014GL059825
Sommers, W. T. (1978). LFM forecast variables related to Santa Ana wind occurrences. *Monthly Weather Review*, *106*(9), 1307–1316. https://doi.org/10.1175/1520-0493(1978)106<1307:LFVRTS>2.0.CO;2
Swain, D. L., Langenbrunner, B., Neelin, J. D., & Hall, A. (2018). Increasing precipitation volatility in twenty-first-century California. *Nature Climate Change*, *8*(5), 427–433. https://doi.org/10.1038/s41558-018-0140-y
Syphard, A. D., Gershunov, A., Lawson, D. M., Rivera Huerta, H., Guzman-Morales, J., & Jennings, M. K. (2018). San Diego wildfires: Drivers of change and future outlook. In M. K. Jennings, D. Cayan, J. Kalansky, A. D. Pairis, et al. (Eds.), *San Diego County ecosystems: Ecological impacts of climate change on a biodiversity hotspot* (pp. 49–69). California's fourth climate change assessment, California Energy Commission. Publication number: EXT-CCC4A-2018-XXX. Retrieved from http://www.climateassessment.ca.gov/techreports/docs/20180827-Biodiversity_CCCA4-EXT-2018-010.pdf
Syphard, A. D., & Keeley, J. E. (2015). Location, timing and extent of wildfire vary by cause of ignition. *International Journal of Wildland Fire*, *24*(1), 37. https://doi.org/10.1071/WF14024
Westerling, A. L., Cayan, D. R., Brown, T. J., Hall, B. L., & Riddle, L. G. (2004). Climate, Santa Ana winds and autumn wildfires in Southern California. *Eos*, *85*, 289–296.
Yue, X., Mickley, L. J., & Logan, J. A. (2014). Projection of wildfire activity in southern California in the mid-twenty-first century. *Climate Dynamics*, *43*(7–8), 1973–1991. https://doi.org/10.1007/s00382-013-2022-3